Supporting Information for the paper: Structure and Dynamics of Model Polymer Mixture Mimicking Levan-Based Bacterial Biofilm of *Bacillus subtilis*

Elizabeta Benigar, Andreja Zupančič Valant, Iztok Dogsa, Simon Sretenovic, David Stopar, Andrej Jamnik, Matija Tomšič

APPENDIX A

Materials. Polysaccharide levan was obtained from biofilm of bacterial organism *B. subtilis* subs. *subtilis* strain NCIB 3610, cultured in a sucrose-rich SYM medium.[1,2] Detailed isolation and purification procedures are described by Benigar et al.[1] DNA was isolated from the cells of the same microorganism, using standard phenol-chloroform extraction protocol. However, due to the complexity and very low yields of isolation of TasA protein from these biofilms,[3] we have used in our study a similar, commercially available protein collagen from calf skin (Sigma Aldrich, BioReagent grade).

All samples were analyzed for their contents of polysaccharides, nucleic acids and proteins spectrophotometrically using the spectrophotometer Thermo Scientific Nanodrop 1000.[1] The EPS matrix of *B. subtilis* subs. *subtilis* strain NCIB 3610 was found to consist from 89.5 wt % of polysaccharides, 4.7 wt % of proteins and 5.7 wt % of nucleic acids. Similarly the composition of isolated and purified levan sample consisted of 98.33 wt % of levan, 0.42 wt % of proteins and 1.25 wt % of nucleic acids.[1] From spectrophotometric ratio A_{260}/A_{280} we found that the purity of DNA was above 99.99 wt % with the protein content of 0.001 wt % determined according to the Bradford method.[4]

Polymer mixtures were dissolved in simple electrolyte solution from SYM growth medium, utilizing strong vortexing. Even though levan samples were prepared as 1, 4, and 8 wt % solutions, DNA samples as 0.06, 0.19, and 0.52 wt % solutions and collagen samples as 0.05, 0.19, and 0.43 wt % solutions, respectively, we focus on 8 wt % levan, 0.52 wt % DNA and 0.43 wt % collagen solutions, as these were the concentrations found in the native biofilm. Polymers were mixed in the same proportions that are found in native *B. subtilis* biofilm.

Rheological measurements. Dynamic rheological measurements were performed on a rotational rheometer Physica MCR 301 (Anton Paar, Graz, Austria) at (20.00 ± 0.01) °C. The rheometer was equipped with the plate-cone measuring system (CP60-0.5/TI) with truncated cone of 60 mm in diameter, angle of 0.52°, and truncation at 62 μm. Oscillatory amplitude sweep measurements were conducted at the angular frequency ω of 10 s^{-1} and the strain γ ranging from 0.05 to 100 % in 21 constant logarithmically-spaced steps, while the oscillatory frequency sweep measurements were conducted at the strain γ of 0.3 % and the angular frequency ω ranging from 100 to 0.05 s^{-1} in 18 constant logarithmically-spaced steps. Due to the limited amounts of samples available, the same measuring system was also used for the rotational viscosity measurements. In this way approximately 1 mL of the sample was sufficient for the measurement, although the sensitivity of the instrument in the rotation mode was somewhat compromised. Viscosity curves at shear rates $\dot{\gamma}$ ranging from 0.1 to 1000 s^{-1} were measured in 25 constant logarithmically-spaced steps with a time delay of 10 seconds between the successive measurements.

Dynamic Light Scattering Measurements. For DLS measurements we used a 3D-DLS Spectrometer (LS Instruments, Switzerland), equipped with a 35 mW He-Ne laser (λ = 632.8 nm). The instrument was used in the 3D-cross-correlation scheme, which eliminates the spurious contribution of the multiple scattering to the DLS data. Samples in cylindrical quartz scattering cells (Hellma; path length of 8 mm) were immersed in a thermostated bath (25 °C) of index matching liquid (decalin). DLS measurements were recorded at scattering angles from 50° to 140° with a step of 10°. Each measurement was 20 seconds long (~500 kHz) and at least 20 of such measurements were averaged to obtain the final autocorrelation function.

The obtained DLS results were interpreted in a sense of the so-called mode coupling theory,[5-7] but since the amplitude of the fast relaxation mode was obviously so low in these samples that could not be resolved from the DLS results, the values of the correlation times τ_c were determined according to the well-known method of cumulants:[8]

$$\tau_c = \frac{1}{D_{\text{eff}} \cdot q^2} \qquad \text{(S1)}$$

where D_{eff} is the effective diffusion coefficient and q is the length of the scattering vector equal to $(4\pi n_s/\lambda)\cdot\sin(\vartheta/2)$, with n_s representing the refractive index of solvent, λ the wavelength of the light, and ϑ the scattering angle. This method yields also the polydispersity index that accounts for the broad distribution of relaxation times in real sample. The obtained results for τ_c were then tested for the nature of the relaxation process in the sample utilizing the plot of $\ln(1/\tau_c)$ vs. $\ln(q)$. For the unconstrained relaxation processes it is characteristic that it is diffusive and the reciprocal value of its correlation time $1/\tau_c$ exhibits the linear dependence on q^2, therefore in such case the slope of a line in $\ln(1/\tau_c)$ vs. $\ln(q)$ equals the value of 2. The mode coupling theory deals with the systems where the scattering moieties strongly interact with their surroundings. Such interactions cause an additional slow

nondiffusive relaxation mode to appear in the DLS results, i.e. due to the coupling effects this slow relaxation shows much stronger q dependence as the diffusive relaxation therefore the slope of the line in $\ln(1/\tau_c)$ vs. $\ln(q)$ is larger than 2. The stronger is the coupling effect the larger value of this slope can be expected and in case of very strong coupling the slow relaxation mode can prevail the DLS signal.[5-7] The slow non-diffusive relaxation mode is therefore typical for polymer systems exhibiting viscoelastic behavior.

Density and Sound Velocity Measurements. The density and sound velocity measurements of sample solutions were performed at 25 °C utilizing the DMA 5005 (prototype instrument; Anton Paar, Graz) equipped with a sound velocity measuring cell. The corresponding adiabatic compressibility values were calculated according to the well-known Laplace equation:[9]

$$\beta_S = \frac{1}{v^2 \rho}, \qquad \text{(S2)}$$

where v is the sound velocity in the solution and ρ the density of the solution. According to the Pasynski model the hydration number n_h can be calculated from these data utilizing the Pasynski equation for dilute solutions:[10]

$$n_h = \frac{n_{H_2O}}{n_{solute}} \frac{(\beta_{S,H_2O} - \beta_{S,sol})}{\beta_{S,H_2O}}, \qquad \text{(S3)}$$

where n_{H_2O} are moles of hydration water molecules, n_{solute} moles of solute molecules, β_{S,H_2O} represents adiabatic compressibility of the water and $\beta_{S,sol}$ adiabatic compressibility of the solution. The hydration numbers given in the present study are expressed as number of hydration water molecules per monomer unit of levan,[1] DNA or collagen.

Microscopy. Microscopy images were taken by the Axio Observer Z1 inverted microscope (Zeiss, Göttingen, Germany), equipped with a 2.5 fold optovar and MRm AxioCam camera using the differential interference contrast technique (DIC). A total magnification of 1000-fold was used. For microscopic examination 5 μL of sample was transferred to a clean glass slide and covered with a cover glass with a thickness of #1.5. Nail polish was used to seal the gap between the slide and a cover glass to prevent evaporation of water. Background images were taken for each sample image. Sample and background images were then processed utilizing ImageJ software (1.48b), which was also used to subtract the background image from the images of samples. A function to enhance the contrast was also used.

Gel Electrophoresis. Gel electrophoresis experiment was performed using 0.8 % agarose gel and 6 × 10 cm mini sub cell GT 8 gel rig (Bio-Rad, Hungary) with a gel volume of 30 mL. Agarose was dissolved in electrophoresis buffer (1× TAE) by microwaving. TAE buffer was also used to cover the gel in the rig. After pouring into a plastic tray with a tape attached to two ends, gel was allowed to solidify at room temperature for at least 20 min. Each DNA sample was mixed with gel loading solution (Sigma Aldrich, Germany) at a ratio 5 : 1 and loaded along with 10 kbp DNA ladder mix (GeneRuler, Thermo Scientific, USA) in the wells in the gel. P25 (Standard Power Pack, Biometra, Germany) power supply was employed for the electrophoresis experiment at 75 V. Electrophoresis was performed until the front edge of the bromophenol blue tracking dye had migrated to a point that was 60 % down the gel. After electrophoresis was completed, gel was stained for 25 min with GelRed Nucleic Acid Red Stain (#41003, Biotium, USA) and rinsed 3–4 times with deionized water. Images were captured using a G: Box (SynGene, UK) gel imager, and edited with GeneSnap software (SynGene, UK).

Small-Angle X-Ray Scattering Measurements and the »String-of-Beads« Model. Small-Angle X-ray Scattering spectra were measured with an in-lab-modified Kratky compact camera (Anton Paar KG, Graz, Austria)[11] at 25 °C. The instrument was equipped with the focusing multilayer optics Osmic MAX-FLUX# as the monochromator. The camera was attached to a conventional X-ray generator PW 3830/00 (Philips-PANalytical B.V., EA Almelo, The Netherlands) equipped with a sealed X-ray tube (Cu K_α X-rays, λ = 0.154 nm) operating at 40 kV and 50 mA. The samples were measured in a standard quartz capillary with an outer diameter of 1 mm and wall thickness of 10 μm for at least 8 hours. The scattered X-ray intensities were detected with a Mythen 1K microstrip solid-state diode-array detector (Dectris, Baden, Switzerland) in the small-angle regime of scattering vectors from 0.065 < q < 7 nm^{-1}, where $q = (4\pi/\lambda)\cdot\sin(\vartheta/2)$. Prior to the further analysis the scattering data were corrected for the empty capillary and solvent scattering and were normalized to an absolute scale using water as a secondary standard.[12] Even though we mark them to be in units of cm^{-1}, we have to point out that the scattering intensities obtained in this way are still experimentally smeared. Such scaling of the experimental SAXS curves is necessary due to the intrinsic smearing procedure of the model used for the SAXS data interpretation. Detailed analysis of the experimental SAXS data was performed utilizing the string-of-beads model described in our previous work.[13-15] To facilitate the reader we explain the model and its application to our data in the following. Within this model the position of the bead relative to its predecessor in the polymer molecule is described by the specific bond angle Θ and torsion angle Φ. When forming the string the excluded volume of the beads is taken into account. In this way different molecular conformations can be simulated. Each pair of angles is denoted as Θ_p and Φ_p, where index p indicates that these specific values are set according to some probability p^* for the random variation of the angles Θ and Φ between the adjacent beads. For example, if $p^* = 0$ all monomer angle pairs Θ and Φ have constant values and the polymer therefore forms a helical structure, but the higher the parameter p^*, the more beads are assigned with random Θ and Φ values, leading to a higher level of randomness in the conformation of polymer molecule (chain). Stiffness of the modeled polymer chain is influenced via parameter Θ_{plim},

which represents the upper limit of the bond angle Θ. Due to the introduction of randomness into the model a specific choice of four shape parameters Θ_p, Φ_p, Θ_{plim} and p^* therefore fully determines a set of similar molecular conformations of the modeled polymer molecule. Prior to the data evaluation these 4 shape parameters are gradually changed in a step-wise manner in a preselected range – the resulting sets of the four shape parameter values determine the entire conformational space of the string-of-beads model as schematically depicted in Figure 1d.[14]

Applying this model to a given polymer the algorithm first calculates adequate representative form factor $\overline{P(q)}$ of the modeled chain for each chosen set of the four shape parameters.[14] Each $\overline{P(q)}$ thus represents the average result for a larger number of molecular conformations related via the individual set of four shape parameters. In the next step of data evaluation each $\overline{P(q)}$ is combined with the term representing the intermolecular interactions forming a total scattering function $I(q)$:[15-17]

$$I(q) = \Delta\rho^2 \left[\frac{8\pi \left\langle \delta\varphi_v^2 \right\rangle \Xi_m^3}{\left(1+q^2\Xi_m^2\right)^2} + \frac{\left\langle \varphi_v \right\rangle v_0}{1+K\cdot e^{-q^2\xi_m^2}} \cdot \overline{P(q)} \right], \quad \text{(S4)}$$

where v_0 is the polymer chain or polymer segment volume, K the constant proportional to the strength of the repulsive interactions, ξ_m the correlation length over which the repulsion occurs, and Ξ_m the correlation length which describes the average size of Debye-Bueche inhomogeneities, which cause the fluctuations in the local volume fraction of the polymer $\left\langle \delta\varphi_v^2 \right\rangle$.[18] The first term in the eq S4 is the classical Debye-Bueche term, which represents the scattering contribution due to attractive intermolecular interactions, which are the reason for formation of Debye-Bueche inhomogeneities. This term depends on the correlation length Ξ_m, which represents the effective size of the dense polymer inhomogeneities within such system. In the second term of eq S4 the form factor of polymer molecules $\overline{P(q)}$ is combined with the classical Debye scattering contribution, which is typical for the system with repulsive intermolecular interactions and depends on the correlation length of the dynamic part of the polymer molecules ξ_m.

Eq S4 can be successfully applied to experimental data in two forms. The first is obtained in the limit assuming that repulsive intermolecular interactions prevail in the model system, which means that $\left\langle \delta\varphi^2 \right\rangle = 0$ and $K > 0$.[15,19] In this case eq S4 simplifies into:

$$I(q) = \frac{\Delta\rho^2 \left\langle \varphi_v \right\rangle v_0}{1+K\cdot e^{-q^2\xi_m^2}} \cdot \overline{P(q)}, \quad \text{(S5)}$$

where the form factor $\overline{P(q)}$ describes the conformations of free polymer molecules in the solution, as dense polymer Debye-Bueche inhomogeneities do not form in such system due to the prevailing repulsive interactions. The second form of eq S4 is obtained assuming that the attractive intermolecular interactions prevail in the model system. This means that $\left\langle \delta\varphi^2 \right\rangle > 0$ and $K = 0$, therefore eq S4 simplifies into:

$$I(q) = \Delta\rho^2 \left[\frac{8\pi \left\langle \delta\varphi_v^2 \right\rangle \Xi_m}{\left(1+q^2\Xi_m^2\right)^2} + \left\langle \varphi_v \right\rangle v_0 \cdot \overline{P(q)} \right]. \quad \text{(S6)}$$

Since the studied solutions of nonionic polysaccharide levan showed considerable elastic character, eq S6 was used also in the present study. The latter choice was reasoned also by the fact that the studied polymer systems were predominantly non-ionic polymer levan systems, therefore the repulsive electrostatic interactions could be neglected. The second term in eq S6 represents the scattering contribution due to the nanostructure of the dense inhomogeneities that is schematically depicted in Figure 1a–c. In this equation correlation length ξ_m is not present, therefore it cannot be obtained in the case of prevailing (attractive) intermolecular interactions in the system. This is also the main reason why the classical correlation lengths[1,20] ξ and Ξ cannot be directly compared to correlation lengths ξ_m and Ξ_m from eq S4, even though their reasoning is very similar.

For the purpose of actual fitting to the experimental data the eq S6 is transformed to equation:

$$I(q) = \frac{A}{\left(1+q^2\Xi_m^2\right)^2} + B\cdot\overline{P(q)}, \quad \text{(S7)}$$

where A, B and Ξ_m are the fitting parameters. In the next step the experimental smearing effects are taken into the consideration by analytical transformation of the Debye-Bueche term[13,20] and by numerical smearing of $\overline{P(q)}$. Then the fitting is performed to the experimental data for every pre-calculated $\overline{P(q)}$, which is representing a specific set of 4 shape parameters Θ_p, Φ_p, Θ_{plim} and p^* in the conformational space. From these fits only the ones with a weighted root mean standard deviation lower or equal to 1 (i.e. better or equal to the experimental uncertainty) are selected as the final result of such modelling.[13-15] The latter is also the reason why the resulting parameters are presented in a form of intervals. Every selected fit namely yields the values of three fitting parameters of eq S7 and corresponds to the set of structure parameters, which are related to an individual $\overline{P(q)}$ that was actually tested in this way. Furthermore, based on the known chemical structure of the polymer one can assess the value of $\Delta\rho^2$ and from the polymer density and geometrical considerations of the model also the value of v_0. These two values are then used to calculate $\left\langle \varphi_v \right\rangle$ and $\left\langle \delta\varphi_v^2 \right\rangle$ from the fitting parameters. Usually they are presented as the ratio $\left\langle \delta\varphi_v^2 \right\rangle / \left\langle \varphi_v \right\rangle^2$.

Interestingly, in practical application of eq S6 we often cannot model the entire polymer molecule, but only its smaller segment composed of N monomers. In fact it turns out that according to this model the appropriate result can be obtained only within a certain range of the segment sizes N,

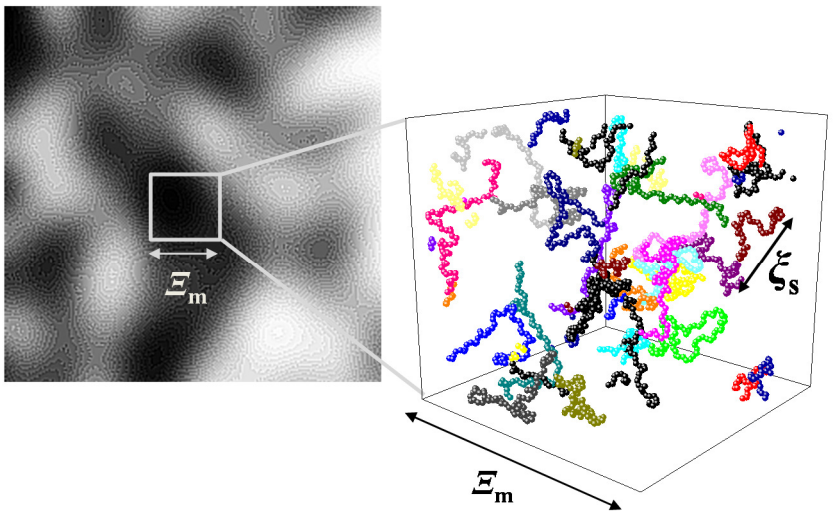

Figure S1: The scheme that illustrates the meaning of the two correlation length parameters: Ξ_m represents the average size of Debye inhomogeneities, while ξ_S ($=2R_g$) represents the size of the simulated polymer segment; each segment of size N is presented in a different color. On the left side of the scheme the black color represents regions of high polymer density and white color the regions of low polymer-density.

which means that the nanostructure of dense polymer inhomogeneities can be described only by mutually uncorrelated segments of certain size N. This is an interesting feature of this model that provides an additional information about nanostructure of the dense polymer inhomogeneities. Polymer segment of size N namely represents the correlated part of the polymer chain within the dense polymer inhomogeneity, i.e. the extent of the intramolecular correlation within the dense polymer correlation length ξ_S, as shown in Figure S1, where dense polymer inhomogeneity is colored in black and low-polymer-density region in white. Correlation length ξ_S thus represents the effective size of the simulated part of polymer chain or the effective size of the segment within dense polymer inhomogeneity, which behaves as an independent intramolecularly correlated structural unit. The value of the correlation length ξ_S is obtained as twice the value of the radius of gyration R_g and is calculated for a segment of N monomers according to the equation:

$$\xi_S = 2 \cdot R_g = \sqrt{\frac{2}{N} \cdot \left\langle \sum_{j=1}^{N} r_j^2 \right\rangle}, \qquad \text{(S8)}$$

where r_j represents the distance of the monomer unit from the center of segment gravity, and angle brackets the average.

This approach to SAXS data evaluation, which has already been successfully applied to a number of ionic and nonionic polysaccharide aqueous systems, can provide some more detailed effective polymer parameters as polymer persistence length, radius of gyration, and correlation length even in the case of micro-phase separated colloidal systems.[13-15,19,21] In the present study we test this approach on dilute and semi-concentrated electrolyte solutions of EPS polymers, different polymer mixtures, as well as on the native and synthetic biofilm systems.

APPENDIX B

Dynamic Light Scattering Results.

The experimental DLS intensity autocorrelation functions of the studied samples are depicted in Figure S2.

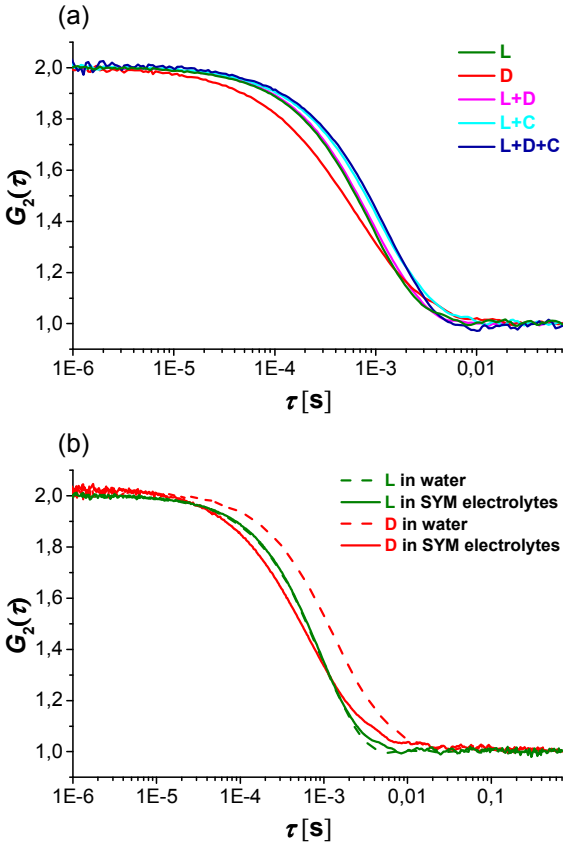

Figure S2. (a) The experimental $G_2(\tau)$ functions measured at the scattering angle of 90° for 1 wt % levan, 0.06 wt % DNA, 0.05 wt % collagen and their mixtures in SYM electrolytes medium and (b) for 1 wt % levan and 0.06 wt % DNA dissolved in water and in SYM electrolytes medium.

Rheological Results.

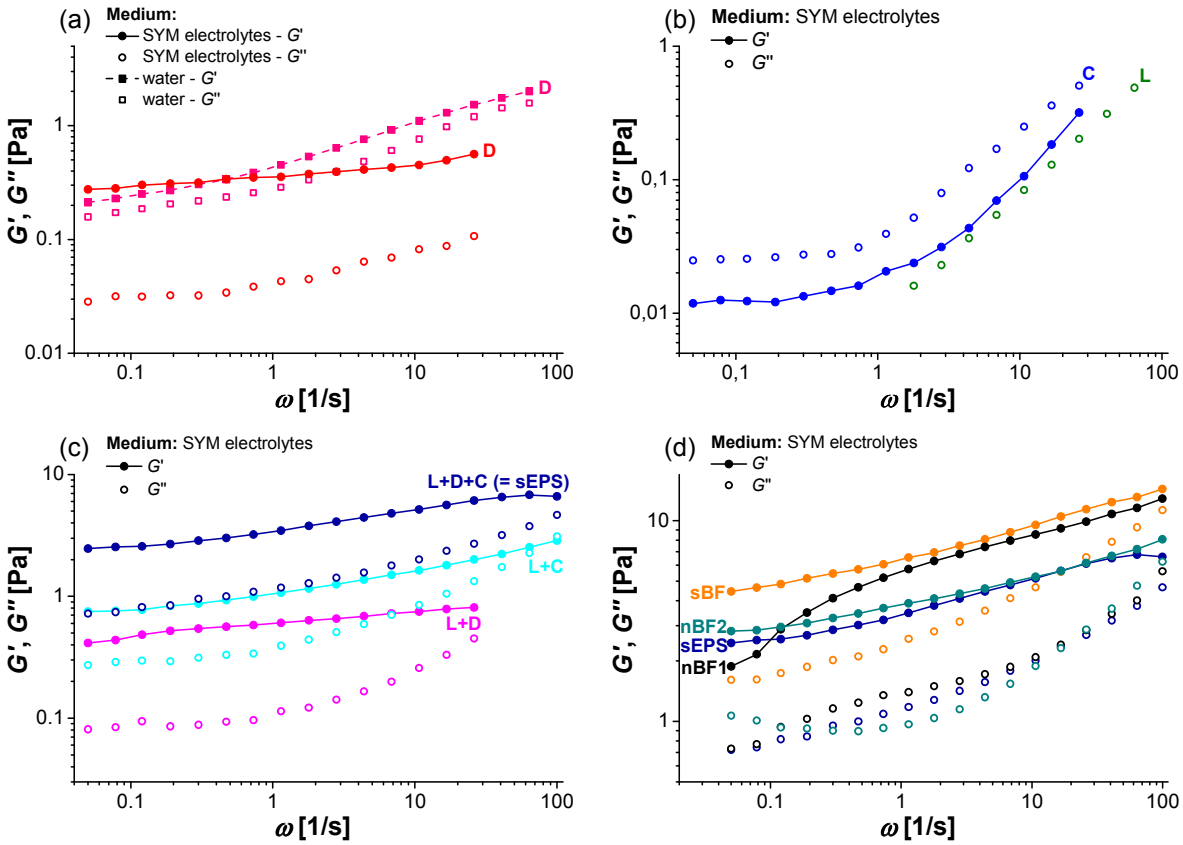

Figure S3. Double logarithmic plot of G' and G'' vs. angular frequency ω for biofilm components and their mixtures measured at 20 °C: (a) The effect of the solvent on DNA solutions, (b) individual biofilm components in SYM electrolytes, (c) polymer mixtures in SYM electrolytes, and (d) comparison of synthetic EPS matrix, synthetic biofilm, native biofilm, and homogenized native biofilm.

Microscopy and Gel Electrophoresis Results.

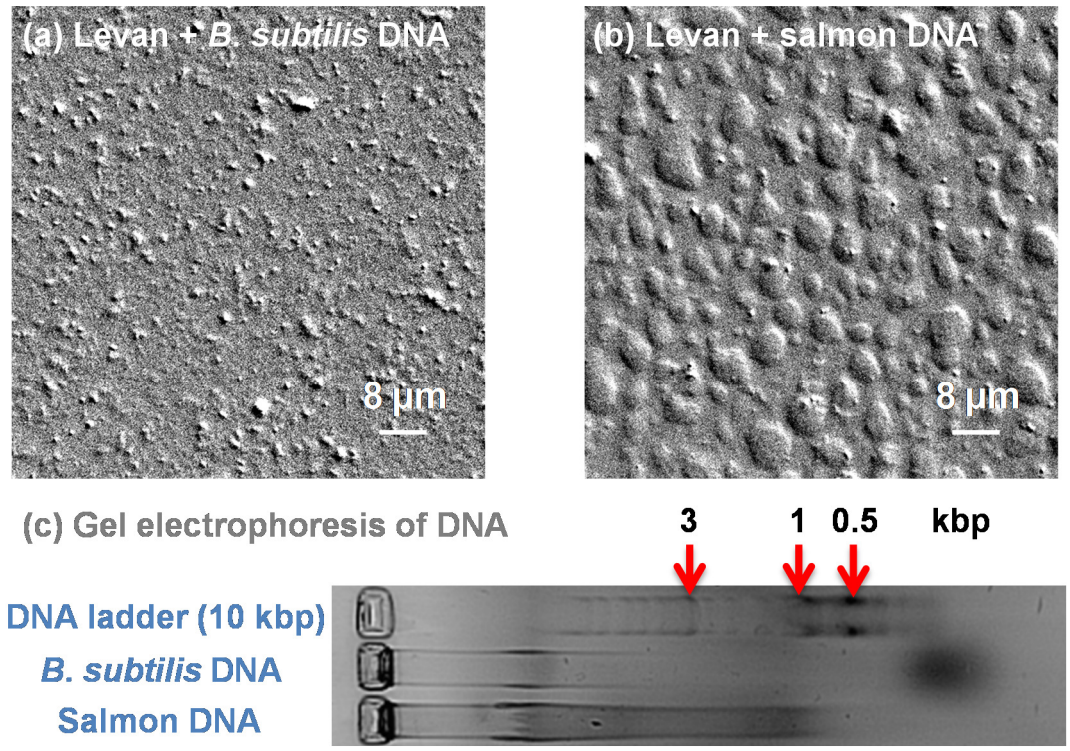

Figure S4. DIC image of (a) 8 wt % levan + 0.52 wt % DNA from *B. subtilis*, (b) 4 wt % levan + 0.23 wt % DNA from salmon, and (c) gel electrophoresis of DNA from *B. subtilis* and DNA from salmon.

Small-Angle X-Ray Scattering Results. In the studied polymer mixture sEPS only levan molecules were modeled. Such simplification could be done since levan molecules are in great majority in these polymer mixture (mass ratio levan : DNA : collagen is 93 : 6 : 5). For samples containing bacterial cells (sBF, nBF1) this model is not suitable, as it cannot properly address the scattering contribution of the cells themselves. Similarly, due to very low polymer concentrations and consequently poor measurement statistic the SAXS data of DNA and collagen binary systems also could not be evaluated this way.

Within the results in Table 1a the difference in the values of segment length N was observed. In this case values of the parameter N do not represent the whole levan molecule, but rather its shorter segment. These values are of course not resulting from the fits, but were obtained by trial and error routine, where different values of the parameter N were tested and the one providing the best fits was selected. It is important to point out that not all of the values of parameter N could provide good fits – if the value was too large there was no satisfactory solution obtained. The two characteristic conformations of modeled molecular segments for levan and sEPS sample are shown in Figure S5.

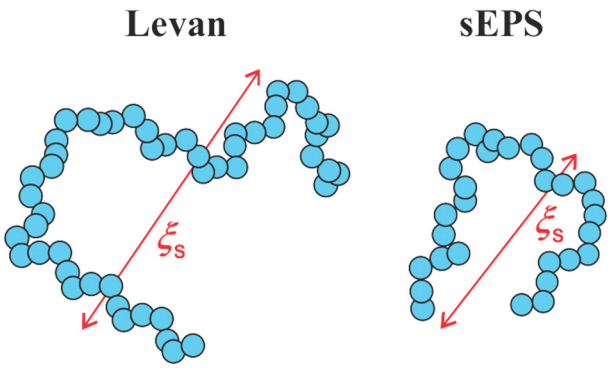

Figure S5. Schematic representation of an example of characteristic modelled polymer segment in levan and eEPS sample obtained by the string-of-beads model.

Results of the string-of-beads model can be further used to visualize the effective Debye-Bueche inhomogeneities.[15] For the case of 8 wt % levan they are shown in a form of subspaces in Figure S6 and are the result of the simulation based on log-normal distributions of number densities of levan, obtained from $\langle \delta\varphi_v^2 \rangle / \langle \varphi_v \rangle^2$ and $\langle \varphi_v \rangle$. For example subspaces denoted by $\varphi_{5\%}$ represent characteristic subspace polymer distribution, found in 5 % of the total sample volume. In subspaces of 8 wt % levan with a side-length of a subspace box 300 Å, there are no major mutual differences observed, except that density of the subspace gradually increases. The differences in the subspace structures of 8 wt % levan sample and sEPS sample are so insignificant that the latter are not shown. This is also due to the fact that the intervals of good fitting solutions for parameter $\langle \delta\varphi_v^2 \rangle / \langle \varphi_v \rangle^2$, which measures the relative fluctuations of local volume fractions and parameter Ξ_m, which measures the scale at which a certain volume fraction is preserved, are

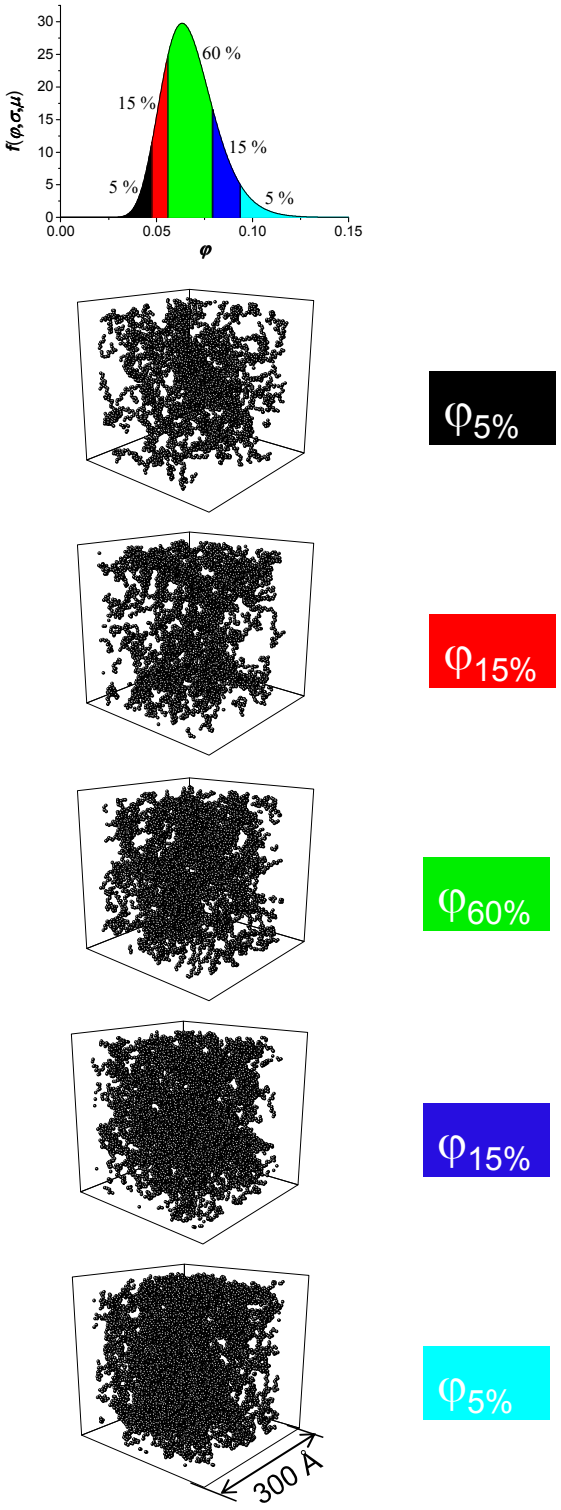

Figure S6: Molecular distribution of 8 wt % levan in space, calculated on the basis of interaction parameters and best fit shape parameters, shown in Table 1. On the right-hand side of the figure the index of φ denotes the probability to encounter a characteristic subspace with the local φ in the levan sample. Estimations: mass density of levan was around 1.45 g/cm^3, the average volume fraction of levan around 6.7 %, and volume of individual segment (N=50) around 9.3×10^{-21} cm^3. The size of a monomer bead (2.6 Å) is shown in proportion to the side length of the subspace box.

for sEPS open upwards. For the parameter Ξ_m fitting algoritem was searching for good solutions in the range of 20

to 1000 Å and good solutions were obtained also at 1000 Å. Extending the search to determine the upper limit of this parameter was not possible, as this would greatly exceed the resolution of SAXS technique. Since the parameter $\left\langle \delta\varphi_v^2 \right\rangle$ is strongly coupled with parameter Ξ_m in eq S6, correspondingly also the solutions of $\left\langle \delta\varphi_v^2 \right\rangle$ and $\left\langle \delta\varphi_v^2 \right\rangle / \left\langle \varphi_v \right\rangle^2$ were not limited upwards.

REFERENCES

(1) Benigar, E.; Dogsa, I.; Stopar, D.; Jamnik, A.; Kralj Cigić, I.; Tomšič, M. Structure and Dynamics of a Polysaccharide Matrix: Aqueous Solutions of Bacterial Levan. *Langmuir* **2014**, *30*, 4172–4182.

(2) Dogsa, I.; Brložnik, M.; Stopar, D.; Mandič-Mulec, I. Exopolymer Diversity and the Role of Levan in *Bacillus subtilis* Biofilms. *PLoS One* **2013**, *8*, 1–10.

(3) Romero, D.; Aguilar, C.; Losick, R.; Kolter, R. Amyloid fibers provide structural integrity to *Bacillus subtilis* biofilms. *PNAS* **2010**, *107*, 2230–2234.

(4) Bradford, M. M. A Rapid and Sensitive Method for the Quantitation of Microgram Quantities of Protein Utilizing the Principle of Protein-Dye Binding. *Anal. Biochem.* **1976**, *72*, 248–254.

(5) Bartsch, E.; Frenz, V.; Baschnagel, J.; Schartl, W.; Sillescu, H. The glass transition dynamics of polymer micronetwork colloids. A mode coupling analysis *J. Chem. Phys.* **1996**, *106*, 3743-3756.

(6) Rajagopal, A. K.; Ngai, K. L.; Teitler, S. Theoretical Aspects of Coupling Model Schemes of Slow Relaxation in Complex Correlated Systems. *J. Non-Cryst. Solids* **1991**, *131*, 282-288.

(7) Kjoniksen, A. L.; Nilsson, S.; Thuresson, K.; Lindman, B.; Nystrom, B. Effect of Surfactant on Dynamic and Viscoelastic Properties of Aqueous Solutions of Hydrophobically Modified Ethyl(hydroxyethyl)cellulose, with and without Spacer. *Macromolecules* **2000**, *33*, 877–886.

(8) Koppel, D. E. Analysis of Macromolecular Polydispersity in Intensity Correlation Spectroscopy - Method of Cumulants. *J. Chem. Phys.* **1972**, *57*, 4814.

(9) Paladhi, R.; Singh, R. P. The Effect of Molecular Weight on Adiabatic Compressibility and Solvation Number of Polymer Solutions. *Eur. Polym. J.* **1990**, *24*, 441–444.

(10) Glinski, J.; Burakowski, A. Modification of the Pasynski Method for Determining the Hydration Numbers of Nonelectrolytes. *Chem. Phys. Lett.* **2013**, *566*, 21–24.

(11) Kratky, O.; Stabinger, H. X-ray Small-Angle Camera with Block-Collimation System an Instrument of Colloid Research. *Colloid Polym. Sci.* **1984**, *262*, 345-360.

(12) Orthaber, D.; Bergmann, A.; Glatter, O. SAXS experiments on absolute scale with Kratky systems using water as a secondary standard. *J. Appl. Crystallogr.* **2000**, *33*, 218-225.

(13) Dogsa, I., Kriechbaum M., Stopar D., Laggner P. Structure of bacterial extracellular polymeric substances at different pH values as determined by SAXS. *Biophys. J.* **2005**, *89*, 2711–2720 .

(14) Dogša, I., Štrancar J., Laggner P., Stopar D. Efficient modeling of polysaccharide conformations based on Small-Angle X-ray Scattering experimental data. *Polymer* **2008**, *49*, 1398–1406 .

(15) Dogsa, I.; Tomšič, M.; Orehek, J.; Benigar, E.; Jamnik, A.; Stopar, D. Amorphous supramolecular structure of carboxymethyl cellulose in aqueous solution at different pH values as determined by rheology, small angle X-ray and light scattering. *Carbohyd. Polym.* **2014**, *111*, 492-504.

(16) Coviello, T.; Maeda, H.; Yuguchi, Y.; Urakawa, H.; Kajiwara, K.; Dentini, M.; Crescenzi, V. Conformational Characteristics of Oxidized Scleroglucan. *Macromolecules* **1998**, *31*, 1602–1607.

(17) Yuguchi, Y.; Mimura, M.; Urakawa, H.; Kitamura, S.; Ohno, S.; Kajiwara, K. Small Angle X-Ray Characterization of Gellan Gum Containing a High Content of Sodium in Aqueous Solution. *Carb. Polym.* **1996**, *30*, 83–93.

(18) Debye, P.; Bueche, A. M. Intrinsic Viscosity, Diffusion, and Sedimentation Rate of Polymers in Solution. *J. Chem. Phys.* **1948**, *16*, 573.

(19) Benigar, E.; Tomšič, M.; Sretenovic, S.; Stopar, D.; Jamnik, A.; Dogša, I. Evaluating SAXS Results on Aqueous Solutions of Various Bacterial Levan utilizing the String-of-Beads Model. *Acta. Chim. Slov.* **2015**, *62*, 509-517.

(20) Cerar, J.; Jamnik, A.; Tomšič, M. Testing Classical Approach to Polymer Solutions on SAXS Data of λ-Carrageenan, κ-Carrageenan and Methylcellulose Systems. *Acta. Chim. Slov.* **2015**, *62*, 498-508.

(21) Orehek, J., Dogša I., Tomšič M., Jamnik A., Kočar D., Stopar D. Structural investigation of carboxymethyl cellulose biodeterioration with *Bacillus subtilis* subsp. *Subtilis* NCIB 3610. *International Biodeterioration and Biodegradation* **2013**, *77*, 10–17.